Available online at www.sciencedirect.com
SCIENCE DIRECT®
Journal of Computational Physics 197 (2004) 647–670
JOURNAL OF COMPUTATIONAL PHYSICS
www.elsevier.com/locate/jcp

A matrix stability analysis of the carbuncle phenomenon

Michael Dumbser [a,*], Jean-Marc Moschetta [b], Jérémie Gressier [c]

[a] *Institut für Aerodynamik und Gasdynamik, Universität Stuttgart, Pfaffenwaldring 21, 70550 Stuttgart, Germany*
[b] *SUPAERO, Department of Aerodynamics, 31400 Toulouse, France*
[c] *ONERA, Department Models for Aerodynamics and Energetics, 31400 Toulouse, France*

Received 26 November 2002; received in revised form 20 October 2003; accepted 10 December 2003
Available online 24 January 2004

Abstract

The carbuncle phenomenon is a shock instability mechanism which ruins all efforts to compute grid-aligned shock waves using low-dissipative upwind schemes. The present study develops a stability analysis for two-dimensional steady shocks on structured meshes based on the matrix method. The numerical resolution of the corresponding eigenvalue problem confirms the typical odd–even form of the unstable mode and displays a Mach number threshold effect currently observed in computations. Furthermore, the present method indicates that the instability of steady shocks is not only governed by the upstream Mach number but also by the numerical shock structure. Finally, the source of the instability is localized in the upstream region, providing some clues to better understand and control the onset of the carbuncle.

PACS: 02.70.Fj; 47.11.+j

AMS: 65M12; 76M25

Keywords: Carbuncle phenomenon; Shock instability; Stability analysis; Numerical shock structure; Riemann solvers; Upwind schemes

1. Introduction

Since shock-capturing techniques have prevailed over shock-fitting methods in the computation of high-speed flows, numerical solutions have been routinely affected by the *carbuncle phenomenon* which is best illustrated by the spurious protrusion ahead of the detached bow shock in the blunt body problem. The carbuncle phenomenon was first reported in 1988 by Peery and Imlay [1] as they computed the supersonic flowfield around a blunt body using Roe's scheme. The carbuncle solution is a stable, entropy-satisfying

* Corresponding author. Tel.: +0049-170-9360238; fax: +0049-711-685-3438.
E-mail addresses: michael.dumbser@iag.uni-stuttgart.de (M. Dumbser), jean-marc.moschetta@supaero.fr (J.-M. Moschetta), jeremie.gressier@onecert.fr (J. Gressier).

0021-9991/$ - see front matter
doi:10.1016/j.jcp.2003.12.013

solution including a recirculating pointed region ahead of the stagnation point. Although it is best illustrated on the blunt body problem, the carbuncle phenomenon occurs in other situations such as the computation of a planar moving shock wave referred to as Quirk's test [2] or the Double Mach Reflection (DMR) problem which consists of a 30° ramp and a moving shock at $M_s = 5.5$. Other carbuncle-like instabilities occur on the steady planar shock wave problem [22], on quasi-conical shock waves around slender bodies and have been also reported in interstellar flow computations in astrophysics [4].

1.1. A physical instability?

The carbuncle solution looks very similar to the one observed experimentally when a very thin spike is introduced along the stagnation line in order to reduce the pressure drag of reentry vehicles [5,6]. Other experiments involving various forms of the bow shock perturbation have shown carbuncle-like pulsating flows. These perturbations include: the injection of a forward-facing jet along the stagnation line [7–9], the injection of dust particles along the stagnation line [10], the energy deposition ahead of the bow shock [11–13]. In many cases, the perturbation yields a pulsating flow which oscillates between the regular detached bow shock and a carbuncle-like shock pattern. As reported in [10], the Strouhal number corresponding to the flow oscillation is relatively independent on the importance of the initial perturbation, suggesting that as soon as it has been triggered, the pulsating flows takes place in a fairly intrinsic manner. For practical applications, in-depth understanding of the carbuncle onset might contribute to provide some clues to monitor shock instabilities in some situations. These shock instabilities can lead to significant pressure drag reduction for blunt body reentry and may prevent the occurrence of local peaks of the wall heat transfer coefficient. From a numerical point of view, the temporal as well as the spatial evolution of the perturbation is consistent with a Jordan form of the perturbation eigenfunctions. Furthermore, it turns out that for several different upwind schemes, namely Roe's scheme, HLLEM and Osher's scheme, there exists a common Mach number value – close to 2.0 – above which the numerical solution destabilizes [14].

Yet, many differences remain between numerical solutions and physical observations, the major difference being that in experiments a certain amount of perturbation (e.g. dust particles [10]) is needed to produce carbuncle-like solutions whereas in numerical computations, round-off errors are sufficient to trigger a shock instability. We will show in the present paper that the numerical carbuncle phenomenon is in fact due to an unconditional instability of the underlying mean flow, so even infinitely small errors will grow exponentially in time if they belong to the unstable modes. Yet, further theoretical and experimental studies should be carried out to investigate the sensitivity of physical shocks to external perturbations.

1.2. Cures for the carbuncle

Most of the time, authors have been focusing on designing cures to get rid of the carbuncle. Apart from multi-dimensional cures, see e.g. [22], a possible cure of the carbuncle by only modifying the quasi one-dimensional flux function is Harten's entropy fix [15] when it is also applied to the eigenvalue associated to the *linear vorticity mode* in Roe's method, resulting in more viscosity in transverse direction, instead of being only applied to the acoustic waves for which it was originally designed and for which it is only physically justified. This immediately leads to a loss of accuracy of the scheme which then no longer exactly preserves steady shear waves, but with this fix, the scheme does not exhibit the carbuncle phenomenon any more [3]. Unfortunately, this correction, even modified to account for directional independency and to reduce the dissipation addition on linear waves, is combined with a tunable pressure sensing function to become active only in the vicinity of shocks [16]. It must be pointed out that even using Harten's entropy fix on the eigenvalue associated to the shear wave, a finite amount of dissipation is needed to damp transverse perturbations since, for instance a typical value of Harten's parameter $\delta = 0.1$ cannot damp perturbations in Quirk's problem while $\delta = 0.2$ removes the odd–even decoupling problem [17]. Similarly, a transverse

velocity component can damp transverse perturbations (see Section 4.3) provided that it has reached a sufficient value. This is the reason why carbuncle solutions may also appear on unstructured grids [18,19] as opposed to Xu's explanation [20].

Actually, in 2D, there are two eigenvalues associated to linear waves: one corresponding to the entropy wave and the other one corresponding to the vorticity wave. As reported in [3,21], it is only the eigenvalue associated to the *vorticity* mode which is responsible for the instability. This confirms that the carbuncle phenomenon is a genuine two-dimensional mechanism since the vorticity wave only exists in 2D. Furthermore, this result is consistent with the stability analysis carried out by Robinet et al. [14] in which the unstable mode precisely corresponds to the vorticity wave. Since the carbuncle phenomenon is a truly two-dimensional mechanism, some authors have proposed to selectively modify the eigenvalues associated to the linear path through multi-dimensional considerations [22]. The idea there is to apply Harten's correction in Roe's method only at particular interfaces located in the vicinity of shock waves. Such a procedure reminds Quirk's proposal [2] which consisted of flagging certain cells where the shock wave is likely to be present and locally applying a dissipative scheme, e.g. HLLE, in the flagged region. In a more recent work Pandolfi and D'Ambrosio [23] have managed to reduce the stencil of interfaces at which a dissipative scheme should be applied while the flagging method is based on the maximum difference of characteristic speeds between two neighboring cells. This approach should be compared to the one suggested by Wada and Liou [24] where instead of considering the maximum difference of characteristic speeds, a sonic point detection is applied.

In all the above carbuncle cures, the onset of instability is thought to be associated to an unfavorable coupling between normal and transverse directions across the shock wave. Yet, the use of a genuinely multidimensional upwind scheme alone does not appear to help for the occurrence of the carbuncle phenomenon [19].

1.3. Numerical parameters which favor the carbuncle

It has been noticed for a long time by the CFD community that no carbuncle appears when the numerical scheme is chosen among the Flux Vector-Splitting (FVS) family. Indeed, FVS schemes naturally diffuse contact waves and damp transverse perturbations in the planar shock problem. The well-known robustness of FVS methods is due to their positivity preserving property; unfortunately, there is no way for a FVS scheme to combine this appealing property with the strict conservation of steady contact waves [25]. Besides the FVS methods, upwind schemes based on the integral approach such as HLLE never produce shock instabilities, except for HLLC in which the conservation of steady contact waves is explicitly restored [26,27]. On the other hand, all schemes which exactly conserve steady contact waves suffer to a certain extent from the carbuncle phenomenon. This empirical observation is consistent with Gressier's linear stability analysis which shows that strict stability on Quirk's test is *incompatible* with the exact resolution of steady contact waves [17]. Strong shock instabilities are routinely obtained using Roe's scheme and Osher's scheme with the inverse ordering of eigenvalues (i.e. the original version). According to Pandolfi and D'Ambrosio [23], HLLC and certain versions of AUSM may produce comparable carbuncle solutions. Weak or mild shock instabilities may still be obtained by the following methods : AUSM-M, AUSM+, HLLC, Godunov and Osher with the natural ordering. Although based on a seemingly different principle, the LDFSS(2) method which exactly preserves steady contact waves also fails on the blunt body problem unless a finite amount of dissipation is explicitly added [29].

Actually, AUSM-M has a very peculiar behavior. Although AUSM-M does not produce a shock instability on Quirk's test, it yields a kinked Mach stem on the DMR problem for sufficiently refined grids [17]. Even on the blunt body problem, AUSM-M as well as AUSM+ may produce mild but clearly visible carbuncle solutions [23] provided that the grid is sufficiently refined and contains elongated cells to favor transverse fluxes. Recent results presented by Liou [28] on the blunt body problem using a more elongated

but less refined grid remarkably confirm that in the blunt body problem, the grid plays a very important role and illustrates the marginal stability of AUSM methods. Furthermore, the marginal stability of AUSM-M is confirmed by the results obtained by Gressier and Moschetta [17] on Quirk's test which shows that AUSM-M cannot damp initial perturbations produced by Roe's method while a FVS method such as EFM does. This seems in contradiction with the claim of a "self-correcting property of the shock-stable scheme AUSM+" made by Liou [28].

Since the exact resolution of steady contact waves is connected to the computation of linear waves, one might think that using the HUS technique would help cure the carbuncle. Indeed, in the HUS strategy, linear waves are computed using a low diffusive method while nonlinear waves, such as shocks, are computed using a robust dissipative scheme [30]. Any two numerical schemes can be combined following the HUS principle to form a resulting hybrid upwind scheme which behaves differently on contact waves and shocks according to the respective properties of either original schemes. Surprisingly, any use of a dissipative scheme such as Van Leer's or EFM [31] for the *nonlinear* waves combined with AUSM scheme for the *linear waves* produces odd–even decoupling in Quirk's problem [3]. This result is rather unexpected since AUSM applied to both types of waves would not produce instabilities in Quirk's test. Furthermore, using AUSM scheme to nonlinear waves guarantees stability on Quirk's tests, no matter what scheme is used for the *linear waves* (even Roe's scheme).

At that point, it seems that as long as an upwind scheme exactly preserves steady contact waves, it will produce somehow a carbuncle solution. However, a new version of AUSM, called AUSMPW+, has been recently proposed by Kim et al. [32] to exactly preserve steady contact waves and simultaneously pass Quirk's test. By the use of pressure-based sensing functions, AUSMPW+ is designed to "suppress even–odd decoupling and carbuncle phenomena", although it is not clear as to what results might be obtained with AUSMPW+ on a fine structured elongated grid for the blunt body problem or on the DMR problem. More recently, the same authors have proposed a modified version of Roe scheme including ad hoc pressure-based sensing functions which drive the rate at which pressure perturbations feed the density field and the rate at which density perturbations are damped out [33]. As a result, two versions of a modified Roe's method are obtained, RoeM1 and RoeM2, which both exactly preserve steady contact waves and pass Quirk's test. Furthermore, it turns out that RoeM2 produces better results than AUSM+ on the DMR problem, confirming that it is even less sensitive to shock instabilities than AUSM+.

1.4. Liou's conjecture

A very puzzling behavior of upwind schemes with respect to the carbuncle phenomenon has been pointed out by Liou who considers that "the root of the multidimensional shock instability, which is manifested by the odd–even decoupling and carbuncle phenomena, is the existence of a pressure term in the mass flux" [28]. More precisely, Liou's conjecture states that if the mass flux of a given numerical flux does not depend on the pressure term for any Mach number, then the scheme will never produce a carbuncle solution. Actually, AUSM method is itself a counterexample of Liou's conjecture since, as observed by several authors [17,23,33], its mass flux does not contain a pressure term while the method may produce shock instabilities in certain situations. Furthermore, there is another counterexample with two kinetic schemes, namely EFM [31] and EIM [34]. Both methods have the *same* mass flux although EFM never produces carbuncle solutions while EIM does [17]. This last result indicates that Liou's conjecture should only apply to numerical methods which exactly preserve steady contact waves. However, in practice, the importance of the mass flux has been clearly illustrated by Liou on Quirk's test [28] and independently confirmed by Moschetta [35] using a quasi-conservative approach which consists of introducing the mass flux of a first scheme into a second scheme. For instance, the use of Godunov's mass flux into AUSM numerical flux actually produces a shock instability on Quirk's test, while a full version of AUSM method does not. Conversely, the use of AUSM mass flux into Godunov's numerical flux does not produce shock

instabilities while the full version of Godunov's method does. Following the same idea, Roe's method can be modified to remove pressure dependency in the original mass flux and this cures shock instabilities through the quasi-conservative method [35].

Unfortunately, directly canceling pressure terms in Roe's mass flux dramatically degrades stability and contradicts a fundamental physical principle according to which a pressure difference *should* create a mass flux, as confirmed by Godunov's exact Riemann solver. As a matter of fact, this relationship is precisely the reason why AUSM is not a positive scheme as shown by Gressier [3].

However, Liou's observation indicates that, even if the carbuncle phenomenon is a 2D shock instability, its origin lies in the 1D formulation of the numerical flux which will be confirmed in the present paper.

1.5. Current explanations for the carbuncle phenomenon

Quirk [2] has been the first one to propose a description for the odd–even decoupling phenomenon starting from the observation that "within the shock, the odd–even decouplings of the pressure and density fields are indeed out of phase with one another". According to Quirk, this will cause "the local sound speed to vary along the length of the shock" and the shock profile to "exhibit a sawtooth perturbation". As a consequence, "the individual segments of the shock will be moving alternately faster and slower than the nominal shock speed" and this movement will then become unstable. Quirk [2] concludes that "any scheme for which it can be shown that the perturbation to the pressure fields feeds the perturbation to the density field will be afflicted by the odd–even decoupling". Although this scenario is very consistent with the observation, it does not explain the origin of the sawtooth perturbations of the density and the pressure fields.

Wada and Liou [24] have also proposed an explanation in which the origin of the carbuncle phenomenon would be "the exchange of information" between intermediate shock points. Section 4.2 of the present paper will confirm this assumption in the sense that intermediate shock points actually play a key role in the onset of the instability.

Finally, Xu and Li [36] have proposed another explanation according to which the subsonic part of the numerical shock profile is the cause for the instability. They suggest that in the subsonic region, pressure perturbations become unstable since "the fluid in the high pressure region will move toward the low pressure region" and "the fluid pressure in the low pressure region will get even lower and the high velocity gets even higher" [36]. This heuristic explanation, if correct, does not prove the *unstable* mechanism involved in the carbuncle mechanism and could even be applied to prove the intrinsic instability of a uniform subsonic flow. However, this explanation points out that the origin of the shock instability lies in the intermediate shock points as in Wada's and Liou's description.

2. The planar steady shock wave instability

Definition 1. In the following, we call a shock *thin* if it is resolved exactly between two cells, whereas a *thick* shock has at least one intermediate point, connecting the upstream and the downstream state.

In [2], Quirk introduced a simplified test in order to get rid of some of the parameters involved in the blunt body problems. Quirk's test consists in calculating the propagation of an unsteady shock wave at $M_s = 6$ in a shock tube of dimension 40×1 on a uniform Cartesian mesh (800×20 cells) which is slightly deformed on the center gridline. Although it is an unsteady test case, it turns out that all numerical schemes which produce carbuncle solutions for the blunt body problem also produce shock instabilities for Quirk's test.

An even simpler problem, which still produces shock instabilities, is the steady normal shock wave problem computed on a 2D grid, proposed by Sanders et al. [22]. This steady shock problem makes stability

analysis much easier. Therefore, Roe's scheme, which is very sensitive to the carbuncle phenomenon, is tried on this simple two-dimensional test problem:

- Calculations are performed on a completely *regular* Cartesian grid, without any grid perturbation, in contrast to Quirk's test where the center gridline in flow direction has been slightly distorted, and also in contrast to the steady planar shock wave test in [22], where one gridline has been distorted in crossflow direction.
- Initial data are given by the exact solution of a normal steady shock wave, obtained from the Rankine–Hugoniot relations. The initial values are submitted to slight random perturbations of the relative order 10^{-6} in all cells and in all conservative variables. The thin shock obtained from the Rankine–Hugoniot relations is located in the middle of the domain.
- The 2D computational domain has the extent 1×1 and contains 25×25 cells.
- The boundary conditions in x-direction are imposed through ghost cells which are constantly set to the exact Rankine–Hugoniot solution, the boundaries in y-direction are periodic.

In 1D, this configuration is stable with Roe's scheme, which resolves exactly thin steady shock waves. Several 2D calculations are now performed in function of the upstream Mach number M_0. The results are the following:

- For upstream Mach numbers below 1.5, the calculation remains stable and the small initial random perturbations decay exponentially in time. This defines a stable zone of upstream Mach numbers (Fig. 1(a)).
- For upstream Mach numbers between 1.5 and 4.6 (Figs. 1(b) and 2), the shock begins to destabilize. In a first phase, the errors grow exponentially in time and form the typical spatial sawtooth pattern (cf. Fig. 2) already described by Quirk. But after some time, the shock has thickened and in a second phase the errors decrease again, converging to a stable thickened steady shock. An explanation of this behavior can be given later with the results of the stability theory developed in this paper, see Section 4.2. In spite of the restabilization process, this range of Mach numbers has to be considered unstable because of the exponential growth of the errors in the first phase.
- For upstream Mach numbers greater than 4.6, the errors grow exponentially in time without a restabilization, leading to the complete destruction of the shock structure. This defines the unstable zone of the Mach numbers (Fig. 1(c)).

Let us note that mesh refinement or coarsening has little influence on the instability threshold between the stable and the deformation zone. Finally, even *without* any spatial and temporal perturbation to the

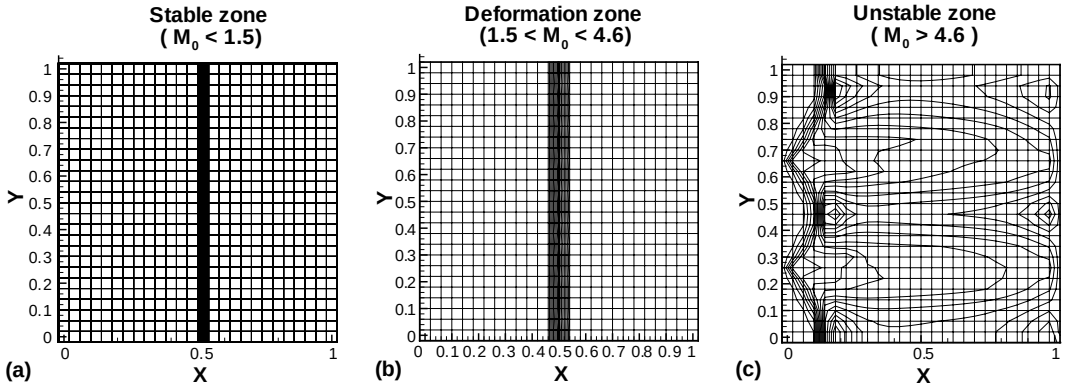

Fig. 1. The different converged flow fields of the steady normal shock wave problem on a regular Cartesian grid in different regions of the upstream Mach number (isodensity contour plots, upstream region: $x < 0.5$, downstream region: $x > 0.5$).

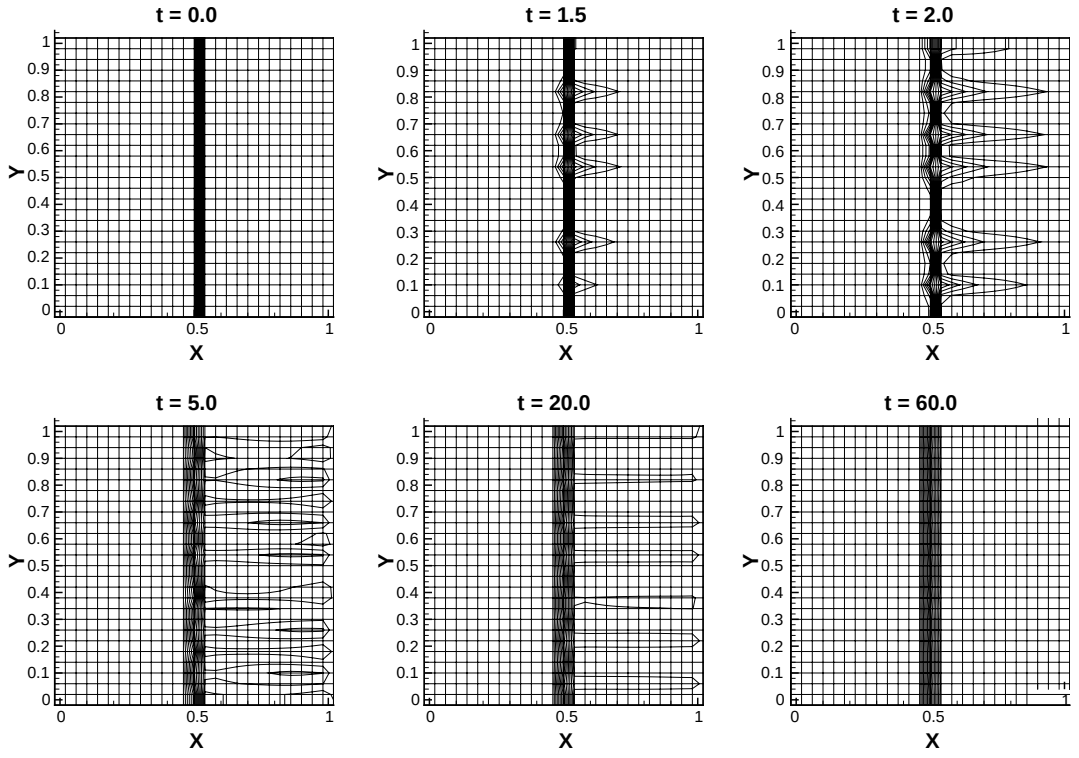

Fig. 2. The thickening process of an initially thin shock at $M_0 = 3.0$.

exact solution, it should be mentioned that Roe's scheme produces instabilities for sufficiently high upstream Mach number values, indicating that round-off errors may be sufficient to trigger the carbuncle.

3. Stability analysis with a matrix-based method

3.1. Governing equations and discretization in space

The fluid considered in this article is modeled by the equation of state of an ideal gas (2) and the inviscid Euler equations (1) in integral form over a control volume Ω and its associated closed surface $\partial\Omega$. The flux vector $\vec{\Psi}$ is written in a local coordinate system (ξ, η) aligned with the unit normal vector $\vec{n} = (n_x, n_y)^{\mathrm{T}}$ pointing outside on the surface element $\mathrm{d}S$

$$\frac{\partial}{\partial t}\int\int\int_{\Omega}\underbrace{\begin{pmatrix}\rho\\ \rho\vec{V}\\ \rho E\end{pmatrix}}_{\vec{W}}\mathrm{d}V + \int\int_{\partial\Omega} M\underbrace{\begin{pmatrix}\rho u\\ \rho\vec{v}u + p\vec{\xi}\\ (\rho E + p)u\end{pmatrix}}_{\vec{\Psi}}\mathrm{d}S = \vec{0}, \tag{1}$$

$$p = (\gamma - 1)\left(\rho E - \frac{1}{2}\rho\vec{V}^2\right), \tag{2}$$

where E is the total energy per mass unit, $\vec{V} = (U, V)^{\mathrm{T}}$ and $\vec{v} = (u, v)^{\mathrm{T}}$ are the speed vectors in global and local coordinates, respectively, and γ is the ratio of specific heats. $\vec{W} = (\rho, \rho U, \rho V, \rho E)^{\mathrm{T}}$ and $\vec{Z} = (\rho, \rho u, \rho v, \rho E)^{\mathrm{T}}$ are the vectors of state written in the global and the local system, respectively, which are coupled by the transformation matrix M as follows:

$$\vec{W} = M\vec{Z} \quad \text{with } M = \begin{pmatrix} 1 & 0 & 0 & 0 \\ 0 & n_x & -n_y & 0 \\ 0 & n_y & n_x & 0 \\ 0 & 0 & 0 & 1 \end{pmatrix}. \tag{3}$$

In the local system, the unit normal vector is simply $\vec{\xi} = (1, 0)^{\mathrm{T}}$. The formulation of (1) in this article uses the property of rotational invariance of the fluxes of the Euler equations.

All the subsequent analysis, which is based on the method explained in [39], is *continuous in time* and thus avoids the influence of time discretization. If any instability was detected by our analysis, it would therefore not only be independent of CFL number but also independent from any time discretization method, because only the spatial discretization operator is being analyzed. The semi-discretized governing Euler equations can be written as

$$\frac{\mathrm{d}\vec{W}_m}{\mathrm{d}t} = \frac{-1}{V_m} \sum_{k=1}^{4} M_{mk} \vec{\Psi}_{mk} A_{mk}, \tag{4}$$

where V_m is the volume of the cell m, M_{mk} is the transformation matrix, A_{mk} the surface of the border between cell m and its neighbor k, $\vec{W}_m$ is the state vector and $\vec{\Psi}_{mk} = \vec{\Psi}_{mk}(\vec{Z}_m, \vec{Z}_k)$ is the numerical flux between two cells with the indices m and k. On a 2D structured grid, each cell m has four neighbors k_1, k_2, k_3, k_4. Eq. (4) contains the continuous temporal evolution of the numerical solution for each cell. For Roe's scheme, for example, the flux function is

$$\vec{\Psi}_{mk}(\vec{Z}_m, \vec{Z}_k) = \frac{1}{2}[\vec{\Psi}(\vec{Z}_k) + \vec{\Psi}(\vec{Z}_m) - |\tilde{J}|(\vec{Z}_k - \vec{Z}_m)] \tag{5}$$

with $\vec{\Psi}(\cdot)$ denoting the exact flux and $|\tilde{J}|$ the absolute value of the Roe-averaged Jacobian matrix $J = \partial\vec{\Psi}/\partial\vec{Z}$.

3.2. Derivation of the stability matrix

For the stability analysis of a steady (time-converged) field, submitted to small numerical random errors, we are interested in the temporal evolution of these errors. The field is expanded into its steady mean value ($\wedge$) and the error (δ)

$$\vec{W}_{m,k} = \hat{\vec{W}}_{m,k} + \delta\vec{W}_{m,k}. \tag{6}$$

The partial derivative of the numerical flux-function with respect to the global vector of state can be written with (3) as

$$\frac{\partial\vec{\Psi}_{mk}}{\partial\vec{W}_{m,k}} = \frac{\partial\vec{\Psi}_{mk}}{\partial\vec{Z}_{m,k}} \cdot \frac{\partial\vec{Z}_{m,k}}{\partial\vec{W}_{m,k}} = \frac{\partial\vec{\Psi}_{mk}}{\partial\vec{Z}_{m,k}} \cdot M_{mk}^{-1}. \tag{7}$$

So the flux function can be linearized around the steady mean value as follows:

$$\vec{\Psi}_{mk}(M_{mk}^{-1}\vec{W}_m, M_{mk}^{-1}\vec{W}_k) = \hat{\vec{\Psi}}_{mk}(M_{mk}^{-1}\hat{\vec{W}}_m, M_{mk}^{-1}\hat{\vec{W}}_k) + \frac{\partial \vec{\Psi}_{mk}}{\partial \vec{Z}_m}\cdot M_{mk}^{-1}\cdot \delta\vec{W}_m + \frac{\partial \vec{\Psi}_{mk}}{\partial \vec{Z}_k}\cdot M_{mk}^{-1}\cdot \delta\vec{W}_k. \tag{8}$$

If the numerical flux function is not differentiable at the mean value in the considered cell, we take the arithmetic mean of the derivatives on both sides of the singular point, see Eq. (19). This will be the case, for example, when calculating the stability of a steady thin shock, which is exactly located on a grid-line, with Godunov's or Roe's scheme. Combining (4) and (6) with (8) and taking into account that the mean-field is *steady*, we finally get the linear error evolution model

$$\begin{aligned}\frac{\mathrm{d}(\delta\vec{W}_m)}{\mathrm{d}t} = \Bigg(&- \sigma_m^{k_1} M_{mk_1} \overline{\left(\frac{\partial \vec{\Psi}_{mk_1}}{\partial \vec{Z}_m}\right)} M_{mk_1}^{-1} - \sigma_m^{k_2} M_{mk_2} \overline{\left(\frac{\partial \vec{\Psi}_{mk_2}}{\partial \vec{Z}_m}\right)} M_{mk_2}^{-1} - \sigma_m^{k_3} M_{mk_3} \overline{\left(\frac{\partial \vec{\Psi}_{mk_3}}{\partial \vec{Z}_m}\right)} M_{mk_3}^{-1} \\ &- \sigma_m^{k_4} M_{mk_4} \overline{\left(\frac{\partial \vec{\Psi}_{mk_4}}{\partial \vec{Z}_m}\right)} M_{mk_4}^{-1} \Bigg)\cdot \delta\vec{W}_m - \sigma_m^{k_1} M_{mk_1} \overline{\left(\frac{\partial \vec{\Psi}_{mk_1}}{\partial \vec{Z}_{k_1}}\right)} M_{mk_1}^{-1}\cdot \delta\vec{W}_{k_1} \\ &- \sigma_m^{k_2} M_{mk_2} \overline{\left(\frac{\partial \vec{\Psi}_{mk_2}}{\partial \vec{Z}_{k_2}}\right)} M_{mk_2}^{-1}\cdot \delta\vec{W}_{k_2} - \sigma_m^{k_3} M_{mk_3} \overline{\left(\frac{\partial \vec{\Psi}_{mk_3}}{\partial \vec{Z}_{k_3}}\right)} M_{mk_3}^{-1}\cdot \delta\vec{W}_{k_3} \\ &- \sigma_m^{k_4} M_{mk_4} \overline{\left(\frac{\partial \vec{\Psi}_{mk_4}}{\partial \vec{Z}_{k_4}}\right)} M_{mk_4}^{-1}\cdot \delta\vec{W}_{k_4}\end{aligned} \tag{9}$$

with $\sigma_m^k = A_{mk}/V_m$ and the notation $\overline{(\cdot)}$ implying an evaluation of the numerical flux-gradient at the steady mean values. The first two lines on the right-hand side of (9) contain the influence of the error in the cell m itself, the last four lines contain the influence of the errors of the four neighbors k of cell m. Eq. (9) has to be written for all cells in the computational domain and so we finally get the error evolution of all $q = N\cdot M$ cells in the domain containing N rows and M columns in matrix notation

$$\frac{\mathrm{d}}{\mathrm{d}t}\begin{pmatrix}\delta\vec{W}_1\\ \vdots \\ \delta\vec{W}_q\end{pmatrix} = S\cdot\begin{pmatrix}\delta\vec{W}_1\\ \vdots \\ \delta\vec{W}_q\end{pmatrix}. \tag{10}$$

In the subsequent sections, we call S the "stability matrix". Eq. (10) assumes that we assign a unique index from 1 to q to each cell in order to identify its influence and position in the stability matrix S.

Considering only the evolution of initial errors, the solution of the linear time-invariant system (10) is

$$\begin{pmatrix}\delta\vec{W}_1\\ \vdots \\ \delta\vec{W}_q\end{pmatrix}(t) = \mathrm{e}^{St}\cdot\begin{pmatrix}\delta\vec{W}_1\\ \vdots \\ \delta\vec{W}_q\end{pmatrix}_{t=0} \tag{11}$$

and remains bounded if the following stability criterion is satisfied:

$$\max(\mathrm{Re}(\lambda(S))) \leqslant 0. \tag{12}$$

Thus, all eigenvalues of S must have negative real parts. The stability matrix has the following form (S_{mk} meaning a submatrix of dimension 4 in the mth submatrix row and the kth submatrix column):

$$S_{mk} = -\sigma_m^{k_1} M_{mk_1} \overline{\left(\frac{\partial \vec{\Psi}_{mk_1}}{\partial \vec{Z}_m}\right)} M_{mk_1}^{-1} - \sigma_m^{k_2} M_{mk_2} \overline{\left(\frac{\partial \vec{\Psi}_{mk_2}}{\partial \vec{Z}_m}\right)} M_{mk_2}^{-1} - \sigma_m^{k_3} M_{mk_3} \overline{\left(\frac{\partial \vec{\Psi}_{mk_3}}{\partial \vec{Z}_m}\right)} M_{mk_3}^{-1} - \sigma_m^{k_4} M_{mk_4} \overline{\left(\frac{\partial \vec{\Psi}_{mk_4}}{\partial \vec{Z}_m}\right)} M_{mk_4}^{-1} \quad \text{if } k = m,$$

$$S_{mk} = \begin{cases} -\sigma_m^k M_{mk} \overline{\left(\frac{\partial \vec{\Psi}_{mk}}{\partial \vec{Z}_k}\right)} M_{mk}^{-1} & \text{if } k \in \{k_1, k_2, k_3, k_4\}, \\ 0 & \text{else} \end{cases} \tag{13}$$

with the set of neighbors $\{k_1, k_2, k_3, k_4\}$ for each cell m and $1 \leqslant m, k \leqslant q = N \cdot M$.

As we want to analyze the stability of a known steady mean-flow, the errors in the ghost cells, which are used to apply the numerical boundary conditions, are set to zero.

4. Applications of the method

4.1. The steady normal shock without structure

4.1.1. Definition of the problem

Eq. (10) shows that the dimension of the stability matrix S is $N \cdot M \cdot 4$ if we apply our method on a 2D structured mesh with $q = N \cdot M$ cells. Application of the stability criterion (12) requires the resolution of the eigenvalue problem for matrix S. Because of its large dimension, the resolution of the eigenvalue problem for matrix S has to be done numerically. For the computations presented in this paper, we used the standard algorithm of MATLAB for computing the eigenvectors and the eigenvalues. Also the gradients of the numerical flux functions are evaluated numerically, which makes it simple to calculate a mean pseudo-derivative if the flux is not differentiable. It is an important point in our method that we use a mean derivative even for non-differentiable schemes. This degrades the quantitative results in prediction of the temporal error growth-rate for non-differentiable schemes, but the main characteristics of the carbuncle phenomenon can nevertheless be retrieved by this method.

First we define a structured uniform Cartesian mesh containing 11×11 cells in the computational domain and including ghost cells along boundaries. The cells are initialized with a thin steady shock on the grid line between the sixth and the seventh column with upstream Mach number $M_0 = 7$. Upstream values are normalized as follows:

$$\vec{W}_0 = \left(1, \quad 1, \quad 0, \quad \tfrac{1}{\gamma(\gamma-1)M_0^2} + \tfrac{1}{2}\right)^{\mathrm{T}} \quad \text{with } \gamma = 1.4. \tag{14}$$

The downstream state $\vec{W}_1$ can be calculated via the Rankine–Hugoniot relations:

$$f(M_0) = \frac{\rho_1}{\rho_0} = \left(\frac{2}{\gamma+1}\frac{1}{M_0^2} + \frac{\gamma-1}{\gamma+1}\right)^{-1}, \tag{15}$$

$$g(M_0) = \frac{p_1}{p_0} = \frac{2\gamma}{\gamma+1} M_0^2 - \frac{\gamma-1}{\gamma+1}, \tag{16}$$

$$\vec{W}_1 = \left(f(M_0), \quad 1, \quad 0, \quad \tfrac{g(M_0)}{\gamma(\gamma-1)M_0^2} + \tfrac{1}{2f(M_0)}\right)^{\mathrm{T}}. \tag{17}$$

The volumes of all cells are equal to unity and because of the Cartesian mesh, the transformation matrices M_{mk} are simply:

$$M_{mk_1} = \begin{pmatrix} +1 & 0 & 0 & 0 \\ 0 & +1 & 0 & 0 \\ 0 & 0 & +1 & 0 \\ 0 & 0 & 0 & +1 \end{pmatrix}, \quad M_{mk_2} = \begin{pmatrix} +1 & 0 & 0 & 0 \\ 0 & 0 & -1 & 0 \\ 0 & +1 & 0 & 0 \\ 0 & 0 & 0 & +1 \end{pmatrix},$$

$$M_{mk_3} = \begin{pmatrix} +1 & 0 & 0 & 0 \\ 0 & -1 & 0 & 0 \\ 0 & 0 & -1 & 0 \\ 0 & 0 & 0 & +1 \end{pmatrix}, \quad M_{mk_4} = \begin{pmatrix} +1 & 0 & 0 & 0 \\ 0 & 0 & +1 & 0 \\ 0 & -1 & 0 & 0 \\ 0 & 0 & 0 & +1 \end{pmatrix}. \tag{18}$$

The stability matrix can then be compiled and its eigenvalues and eigenvectors be calculated. The gradients of the numerical flux function are evaluated numerically with a centered approximation

$$\frac{\partial \Psi_i}{\partial Z_j} \approx \frac{\Psi_i(Z_j + \Delta Z_j) - \Psi_i(Z_j - \Delta Z_j)}{2\Delta Z_j}, \quad i, j \leqslant 4 \tag{19}$$

providing an average of the derivative for non-differentiable schemes. More sophisticated methods according to [38] have also been tried to tackle non-differentiable non-linear systems under random perturbations, but did not yield better results than our simple approach presented above. In Eq. (19), Ψ_i is the ith component of the numerical flux provided by the scheme where we have dropped the cell indices m and k for clarity and Z_j denotes the jth component of the state vector (written in the local coordinate system) in the cell m and the neighbor k, respectively.

All computations presented in this paper have been carried out in MATLAB using $\Delta Z_j = 10^{-6} = \text{const}$. Other values of ΔZ_j in the range of 10^{-2}–10^{-8} have also been tried on the example of Roe's and Osher's schemes with a shock at an upstream Machnumber of $M = 7.0$. The effect of this variation on the unstable eigenvalue is summarized in Table 1 and supports our choice.

Although only applied in this paper to a uniform Cartesian grid, the presented method can be easily extended to more general 2D grids including unstructured grids, provided that a steady reference solution for these grids can be found.

4.1.2. Results

The stability of the following schemes has been analyzed: Godunov, Roe, EFM, Van Leer, HLLE, HLLEM [37], Osher and AUSM-M. The eigenvalues of the stability matrix of the steady shock problem at $M_0 = 7$ are shown in Fig. 3. The schemes presented on the left, which exactly conserve steady contact discontinuities and which are all well known to produce the carbuncle phenomenon, have multiple eigenvalues with positive real parts which evidently lead to an unstable behavior. The schemes on the right, known to add numerical dissipation on steady contact discontinuities except for AUSM-M, have always eigenvalues with negative real parts, demonstrating their stability. Nevertheless the AUSM-M scheme holds a particular position because the largest real part is nearly zero up to the accuracy of the algorithm which

Table 1
Influence of the numerical differentiation on the unstable eigenvalue

	ΔZ_j	10^{-2}	10^{-3}	10^{-4}	10^{-5}	10^{-6}	10^{-7}	10^{-8}
Roe	$\max(\mathrm{Re}(\lambda))/10^{-1}$	7.391	7.412	7.414	7.414	7.414	7.414	7.414
Osher	$\max(\mathrm{Re}(\lambda))/10^{-2}$	7.509	8.163	8.229	8.235	8.236	8.236	8.236

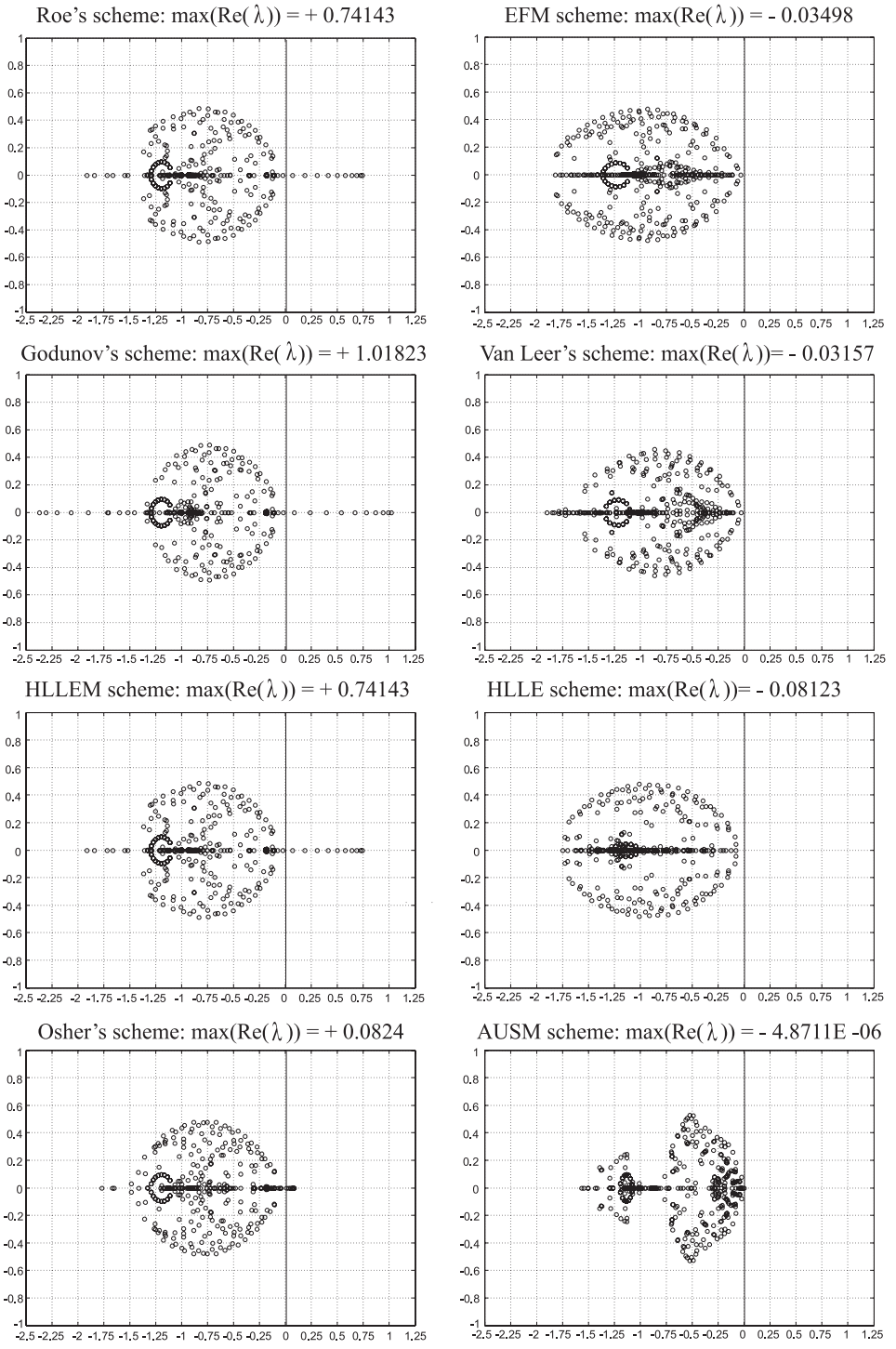

Fig. 3. Distribution of the eigenvalues of S in the complex plane for different schemes according to the stability theory (grid with 11×11 cells, upstream Mach number $M_0 = 7.0$). Unstable schemes with $\max(\mathrm{Re}(\lambda)) > 0$ are in the left column, stable schemes are in the right column.

calculates the eigenvalues. It has therefore to be considered as marginally stable according to our theory, even if in practice it is stable in Quirk's test and does not produce the plane wave instability. The special position of AUSM-M among the numerical schemes is also clearly visible in the distribution of the poles of S, which completely differs from those of the other schemes (Fig. 3).

If we now look at the most unstable eigenvalue of S (for example considering Roe's scheme), the corresponding eigenvector contains the information of the spatial-behavior of the unstable mode. It is well known that the carbuncle instability exhibits a sawtooth-like form (cf. [2]) in the transversal direction (y axis) which is correctly predicted by our theory (cf. Fig. 4) and qualitatively confirmed in numerical experiments. We would like to note that the unstable mode presented in Fig. 4 is exponentially decaying in normal direction (x axis). As shown in Fig. 4, the upstream region does not appear to participate in the unstable behavior, except for the column of upstream cells directly adjacent to the shock. This important point will be discussed later. The unstable eigenvalues seen in Fig. 3 are all on the real axis, which means an exponential growth of the instability, without oscillation (cf. Eq. (11)).

In Fig. 5 we show the evolution of the norm $\|V\|_\infty(t)$ of the transverse velocity, which is a direct measure of numerical errors since the exact solution is known to be $V = 0$ for the mean flows analyzed in this section. The numerical experiment to obtain Fig. 5 was performed with Roe's scheme on a thin steady normal shock at $M_0 = 10$. In the time interval from 0 to 2, which we call the initial transition region, the

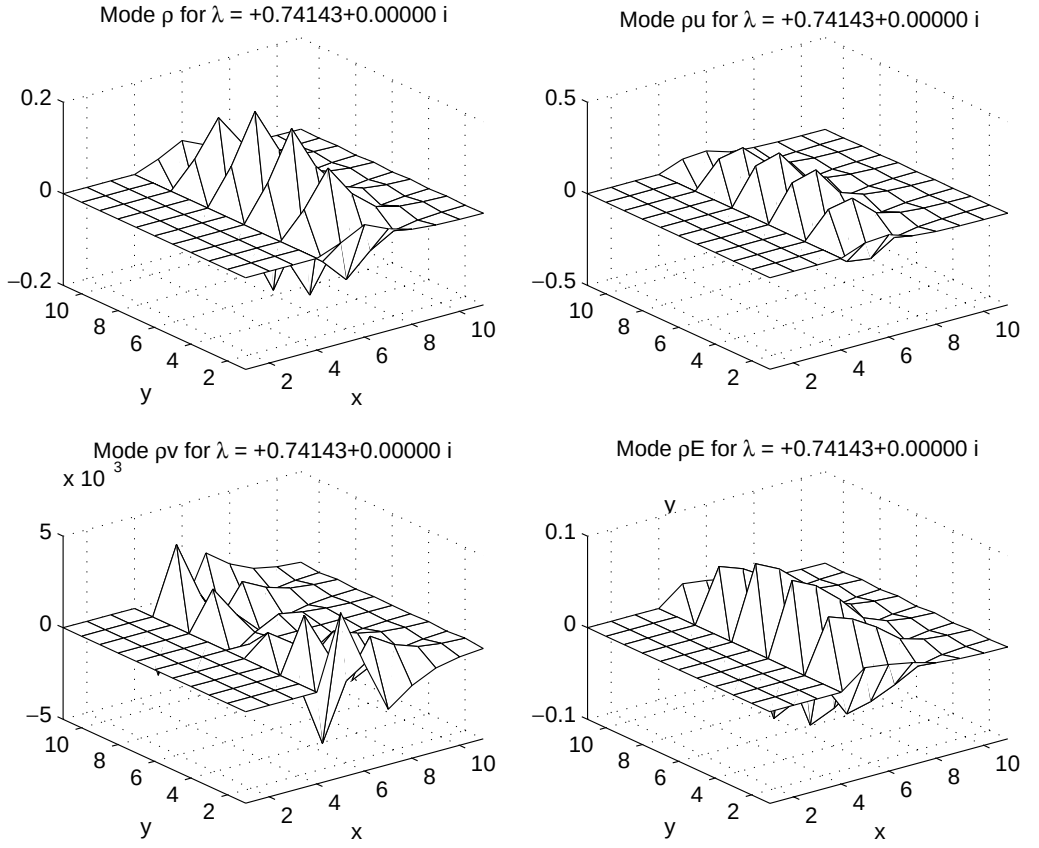

Fig. 4. Theoretical prediction of the sawtooth form of the unstable mode in Roe's scheme.

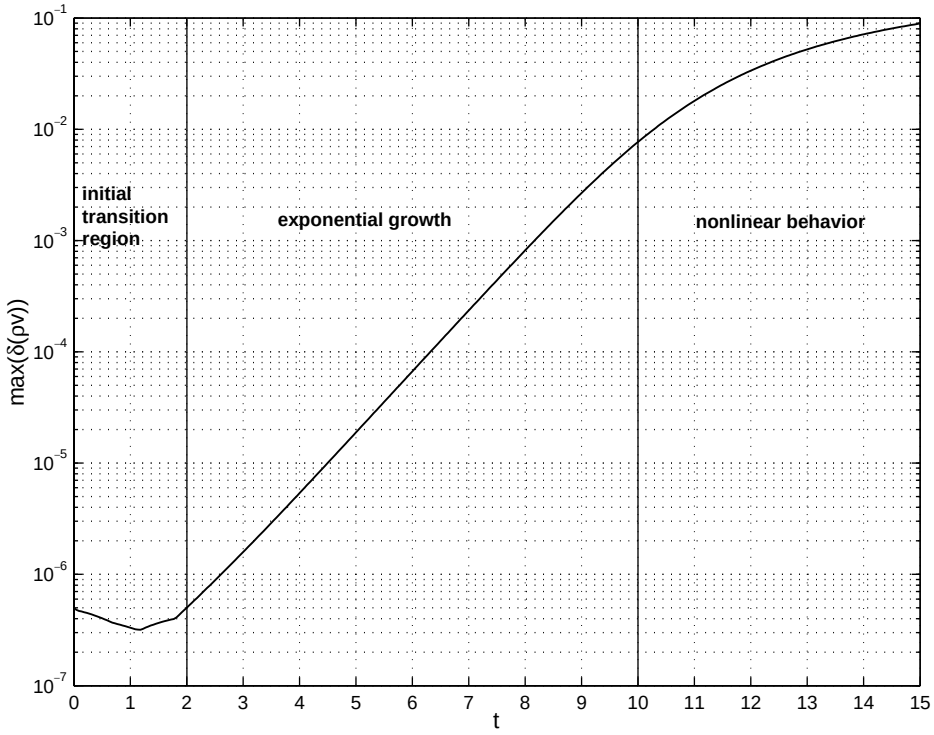

Fig. 5. Exponential growth of the error δv, initial and nonlinear behavior obtained in a numerical experiment with Roe's scheme at $M_0 = 10$.

errors decrease in time. This might be due to the damping of stable modes. The time interval from 2 to 10 shows clearly an exponential growth of numerical errors. From this linear part of Fig. 5 we deduce that the errors obey an exponential law of the form

$$\|V\|_\infty(t) = V_0 e^{\lambda_{\text{num}}(t-t_0)} \tag{20}$$

in this time interval. For all numerical experiments, the parameters V_0, t_0 and λ_{num} can be directly determined (e.g. with a least-squares technique) from the linear part of a semi-logarithmic plot, such as the one shown in Fig. 5. In the following, we call λ_{num} the temporal error growth rate. This temporal error growth rate can now quantitatively be compared to the prediction $\max(\text{Re}(\lambda))$ of the stability theory, which gives the theoretical temporal error growth rate of the most unstable mode according to Eq. (11).

When the errors become sufficiently large, nonlinear effects play a role and lead away from exponential growth which can be observed in Fig. 5 in the time interval from 10 to 15.

The quantitative validation is best performed with a differentiable scheme for which the linearization (8) holds exactly. The two versions of the Osher scheme are for example differentiable due to their particular integral formulation. For validation purposes, we compare the maximum real part of the eigenvalues of S (theory) for different upstream Mach numbers with the temporal error growth rate in numerical experiments. As Osher's scheme generally does not exactly conserve thin shocks in 1D, the mean reference flow around which the linearization (8) is performed has to be calculated beforehand. An initially thin shock is placed in a 1D domain, then a 1D computation is performed up to time convergence and the resulting steady field, which contains a thickened shock, is projected onto the 2D domain. This technique has already

been applied by Sanders et al. [22] to obtain initial conditions for their numerical experiments. Then the stability matrix can be calculated as described above. We note that this process of shock thickening with the Osher scheme (and also EFM, Van Leer, AUSM-M, etc.) is related directly to the one-dimensional flux functions of these schemes, which do not conserve thin steady shocks. This kind of thickening has nothing to do with the unstable shock thickening of a 2D thin shock when using Roe's scheme, as shown in Fig. 2. Fig. 6 shows a very good agreement between theoretical prevision and experiments in the unstable Mach region. In the stable region, the theory predicts a temporal error-decreasing rate which is slower than the true one observed in computations. Fig. 6 reveals furthermore an interesting difference between the two versions of Osher's scheme. Both versions become unstable if a threshold value in the upstream Mach number of about 2.3 is exceeded. But whereas the inverse order version remains unstable, the natural order version suddenly becomes stable again at an upstream Mach number of 5.5. The explanation for this particular phenomenon will be given in Section 4.4. For non-differentiable schemes like Godunov's and Roe's, the present method is not able to quantitatively predict neither the temporal growth of the instability nor the destabilization threshold value. Fig. 6 shows clearly an important error in the theoretical prevision due to non-differentiability. Only the order of magnitude is correct. It is important to notice that the stability theory underestimates the growth rate because of averaging the derivatives on both sides of the non-differentiable point. We can see that for a quantitative error analysis, the technique of using a mean-derivative is not adequate. Section 4.2 will show that we can better handle the thin shock case as a limit of the case with an internal numerical shock structure. Nevertheless it is the first stability analysis of the semi-discretized Euler equations which is really able to predict an unstable behavior of certain numerical schemes. This instability will lead to the carbuncle phenomenon for stationary straight shocks.

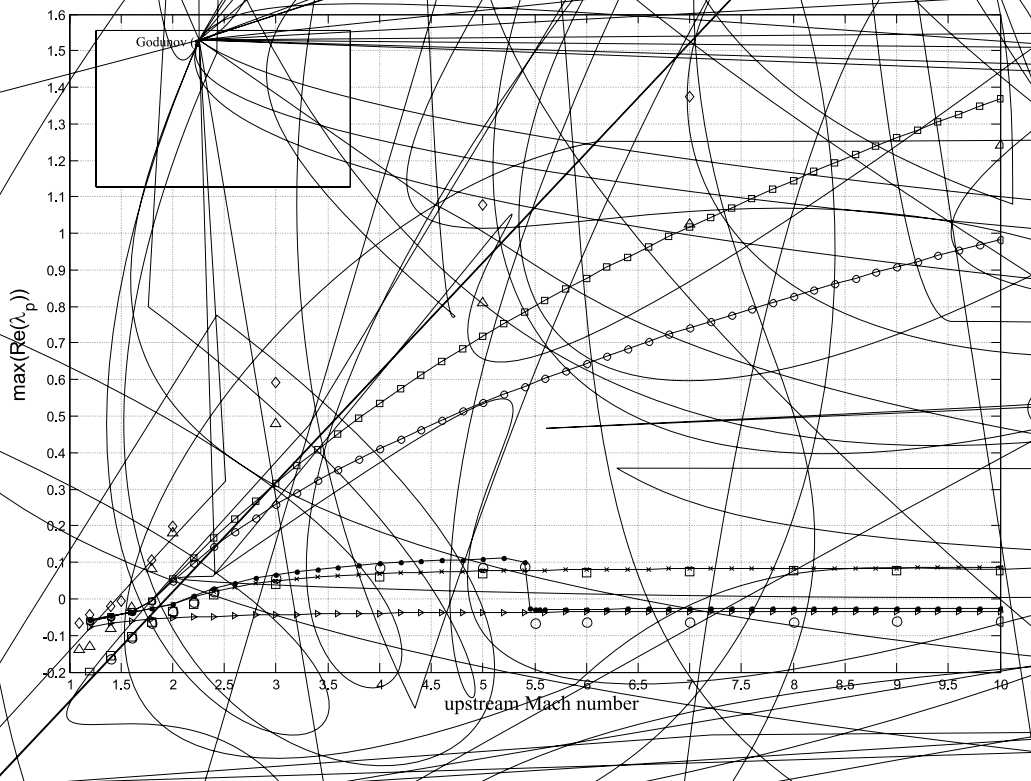

4.2. The steady normal shock with numerical shock structure

In Section 2, using Roe's scheme, we have seen in Fig. 1(b) that there are situations where the shock destabilizes, thickens and the so thickened shock becomes stable again. The observations reported in Section 2 have suggested a closer investigation of the numerical shock structure. A linear stability analysis for viscous shock profiles has already been done by Sanders et al. [22]. They used a generic truncation error equation which did not take into account all the properties of the different two-point upwind schemes. Our approach is based on a direct linearization of the numerical flux function which allows us to distinguish between the different Riemann solvers.

It is known that Roe's scheme exactly conserves thin steady normal shock waves, but if an intermediate point is introduced, the solution converges to a thick shock which keeps an intermediate state, though different from the initial one. Let us define the initial intermediate state $\vec{W}_i^0$ as a linear combination of the upstream and downstream states

$$\vec{W}_i^0 = \alpha_0 \cdot \vec{W}_0 + (1 - \alpha_0) \cdot \vec{W}_1, \quad 0 \leqslant \alpha_0 \leqslant 1. \tag{21}$$

The upstream and downstream states are determined by the upstream Mach number and the Rankine–Hugoniot conditions. Fig. 7 presents different 1D converged shock structures with an intermediate point, dependent on the initial form factor α_0, showing the non-uniqueness of the solution. One can distinguish between shocks with convex and shocks with concave structure. We now project these time-converged 1D shock structures on a 2D grid and perform a stability analysis for different values of the upstream Mach number and of the form-factor α_ρ. This form factor, which is different from the initial factor α_0, is defined as

$$\alpha_\rho = \frac{\rho_i^c - \rho_1}{\rho_0 - \rho_1}, \tag{22}$$

where ρ_i^c is the converged density of the internal shock point. The results of the stability analysis are plotted in Fig. 8. We first note that the convex shocks ($\alpha_\rho < 0.5$) are generally more stable than the concave ones ($\alpha_\rho > 0.5$). Second, the greater the Mach number the closer the curves get (see the small distance between

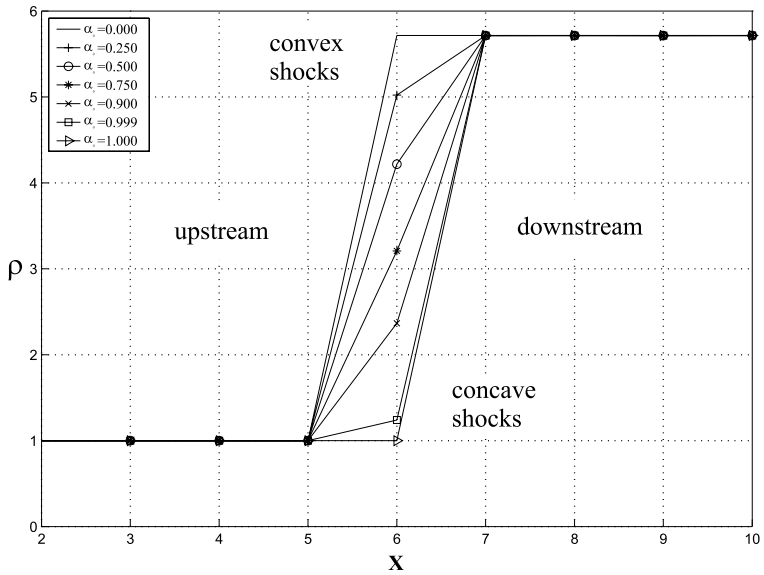

Fig. 7. Different converged 1D shock structures dependent on the initial form factor α_0 (Roe's scheme at $M_0 = 10.0$).

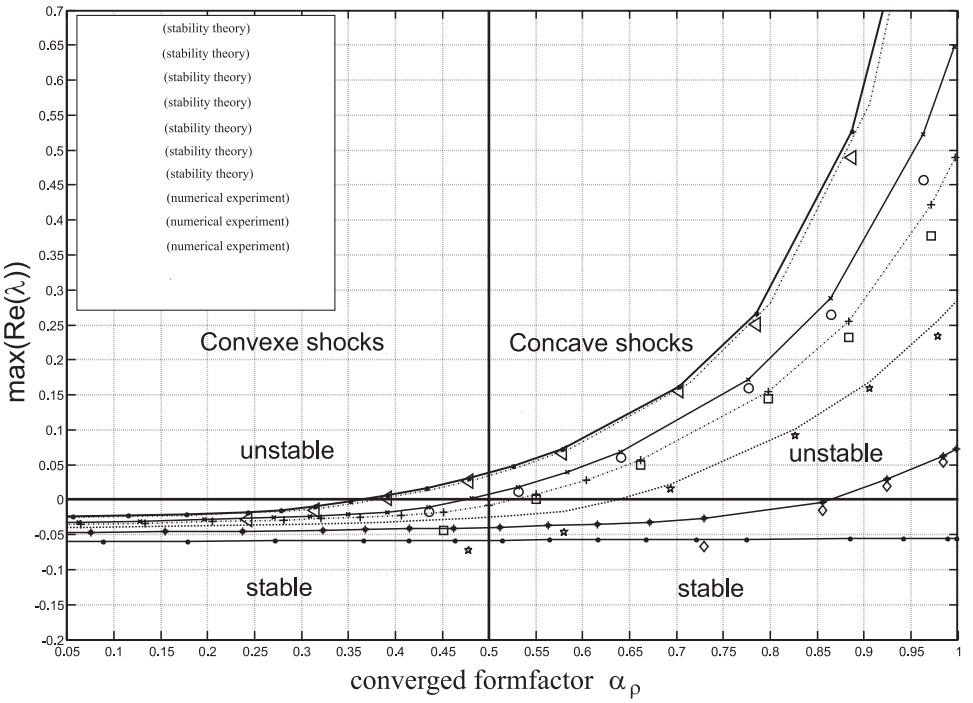

the $M = 10$ and the $M = 100$ curves), so the temporal error growth rate gets limited for very large Mach numbers. Third, very convex shocks ($\alpha_\rho < 0.35$) are stable for any value of the upstream Mach number (theoretical analysis and experiments cover upstream Mach numbers up to 100). Fourth, the shock remains stable independently of the form only for very small Mach numbers (below 1.5). An important point is also that for thick shocks, the eigenvalues of the Roe-averaged Jacobian matrix are all non-zero and so the flux becomes differentiable around this mean flow, which explains the good agreement between theoretical prediction and the temporal growth rate found in numerical experiments. This provides a method to handle the thin shock case as the limit ($\alpha_\rho \to 1$) of the case with shock structure.

Remark 2. Of course, the two limit cases $\alpha_\rho \to 1$ and $\alpha_\rho \to 0$ both represent the thin steady normal shock, only with a phase difference of one cell. If we carry out our stability analysis directly in the limits of one and zero (having to face the problems of non-differentiability), the values of the largest real parts of the stability matrices are in both cases almost the same. But the calculated values are continuous only in the case $\alpha_\rho \to 1$ and form a highly discontinuous jump from stable to unstable in the case $\alpha_\rho \to 0$. This is the reason why we define the behavior of the thin steady shock as a limit of the case $\alpha_\rho \to 1$. For Roe's scheme, the thin shock "inherits" the unstable properties of the concave shocks.

These observations give clues to better understand the scenario of shock thickening presented in Fig. 1 for Roe's scheme. For very small upstream Mach numbers (below 1.5), Fig. 8 predicts overall stability of the shock, independent of its form. For higher upstream Mach numbers, a thin steady shock becomes unstable (Fig. 8) but the developing numerical shock structure may trigger the restabilization process shown in Fig. 2 in the convex case, or leads to unbounded growth of the numerical errors in the concave case.

The analysis of the influence of the numerical shock structure provides new insight in the mechanism which generates the carbuncle. The assumption of Wada and Liou [24] that the internal points of the numerical shock structure exchange information and generate the instability has now been quantified and is thus supported.

4.3. Influence of grid distorsion and transverse velocity

Concerning mesh distorsion, we consider the case that the meshsize in x-direction remains constant $\Delta x = 1$. The total number of grid cells remains the same for all analyzed meshes. We then define a distorsion factor

$$\delta = \frac{\Delta y}{\Delta x} \tag{23}$$

and compute the eigenvalues of S in function of δ and some Mach numbers for Osher's scheme (IO) on a grid consisting of 11×11 cells. The theoretical results are corroborated by numerical experiments. We assume periodic boundary conditions in y-direction. Fig. 9 shows the maximal real part of the eigenvalues of S as a function of δ. One can clearly see that the shock wave instability is highly damped when the grid becomes more and more elongated in y-direction and that it can even be damped out completely if the grid is sufficiently distorted, depending on the upstream Mach number. It is also obvious from Fig. 9 that perturbations grow faster when the grid is refined in y-direction, as found by Pandolfi and D'Ambrosio [23] in the blunt body case. Similar results are obtained when the extent of the computational domain is fixed and the number of cells in y-direction is increased or decreased.

Another important factor which influences the carbuncle phenomenon and which also arises in the blunt body case is a transverse velocity component. Up to now, we simply studied the two-dimensional stability

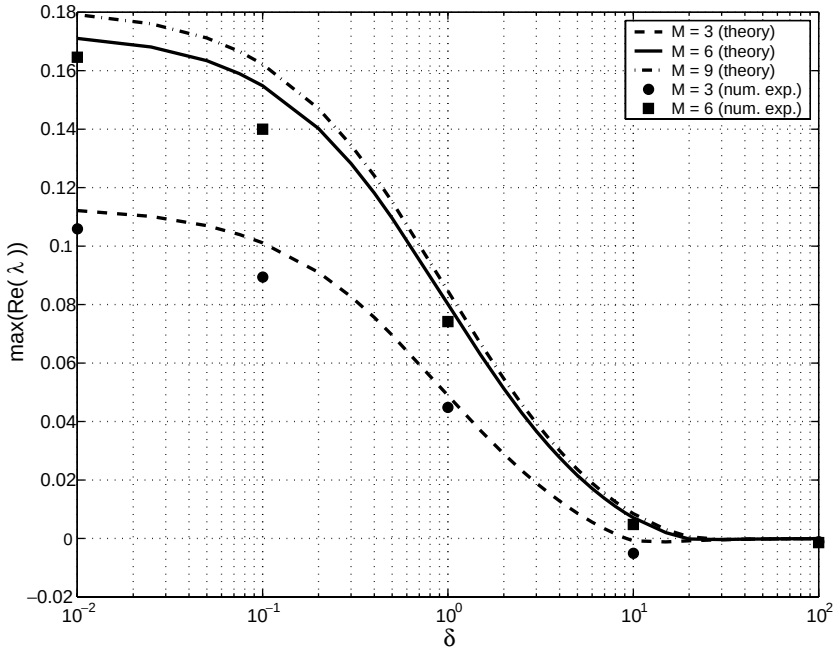

Fig. 9. Influence of grid distorsion and Mach number on the instability (Osher's scheme (IO), 11×11 grid, $\Delta x = 1$).

of a purely one-dimensional flowfield. In the following we add a non-zero component V to the velocity vector using as parameter the angle

$$\tan\phi = \frac{V}{U}. \tag{24}$$

The results of the stability analysis are presented in Fig. 10 from which we deduce that the shock instability vanishes if a certain threshold, which depends on the upstream Mach number, of the transverse velocity is depassed.

With these findings we can conclude that the steady planar shockwave problem [22] is well suited as a model problem for studying separately the influence of several parameters which jointly intervene in the blunt body case such as mesh distorsion, transverse velocity and upstream Mach number.

4.4. Spatial localization of the source of instability

The matrix stability theory allows to include boundary conditions in the analysis which will be useful to figure whether the carbuncle phenomenon originates from the upstream or from the downstream side. For this purpose, two test cases which both apply to thin shocks have been set up. In the first one (Fig. 11(a)) we put a thin steady normal shock exactly on the upstream boundary. So the ghost cells on the left are set to the upstream state $\vec{W}_0$ while all other cells are set to the downstream state $\vec{W}_1$. The boundaries are supposed to be error-free, so their direct contribution to error evolution vanishes in the stability matrix except from the flux-gradient, which includes the shock. This procedure prevents any errors to develop in the upstream region and we can hence analyze the stability of the downstream region separately, but still taking into account the presence of the shock. In the second test case (Fig. 11(b)) we put the steady shock on the downstream boundary, thus suppressing any errors in the downstream region. This setup will grant insight

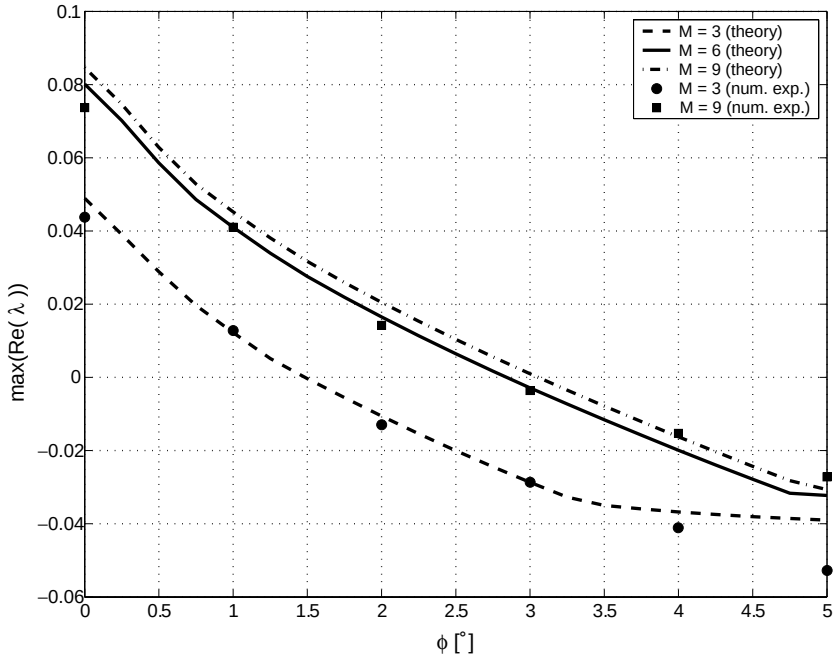

Fig. 10. Influence of transverse velocity and Mach number on the instability (Osher's scheme (IO), 11×11 grid).

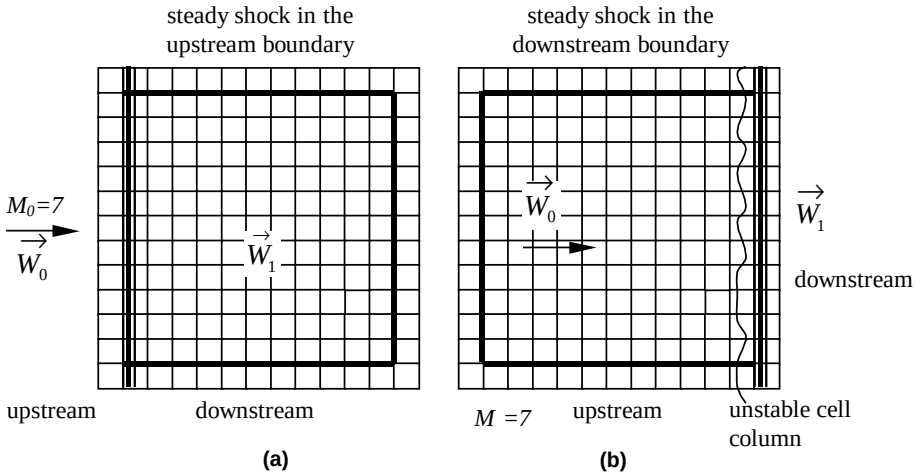

Fig. 11. The upstream and the downstream testcase.

into the stability behavior of the upstream region in the presence of a shock. Analysis is performed for Roe's scheme at $M_0 = 7$.

The results for both test cases can be summarized as follows. In the case of the shock on the upstream boundary, the stability theory predicts a stable behavior ($\max(\mathrm{Re}(\lambda)) = -0.039$), if the shock lies on the downstream boundary, the theory predicts an unconditional instability ($\max(\mathrm{Re}(\lambda)) = +0.25$). Taking a look at the spatial behavior of the unstable mode in the second test case, the eigenvectors of the stability matrix S reveal that only the cell column directly adjacent to the shock on the upstream side (Fig. 11(b)) participates in the instability but not any further cells in upwind direction. This is obvious because of the upwinding character of Roe's scheme. The theoretical results have been confirmed by numerical experiments. So we can draw the following conclusions: The shock instability does not originate from the downstream region, as supposed by Xu [20]. In the case of a thin shock, the instability arises only from one single column of upstream cells, directly adjacent to the shock. The unstable mode which can be seen in the downstream region (Fig. 4) is only the convected result, not the cause of the instability, which lies upstream.

In order to further support the importance of the upstream region, without having the effect of the boundary conditions, we analyze the stability of a thin shock in the middle of the computational domain with a modified numerical flux for the upstream cells directly adjacent to the shock. When the numerical flux is artificially set to the exact upstream flux on the cell interface which contains the shock, the instability vanishes in both the stability theory and in computations, thus emphasizing the important role of the upstream region in the generation of the carbuncle. This last result provides a clue to explain the surprising behavior of Osher's scheme shown in Fig. 6. Above $M_0 = 5.5$, the natural order version of the Osher scheme captures exactly thin steady normal shocks because both intermediate Osher states become supersonic, which sets the flux at the shock interface equal to the exact upstream flux, see Fig. 12 which shows the relative error in the numerical mass flux for a thin shock compared to the exact flux. A similar behavior is obtained for the fluxes of momentum and total energy. This peculiar property can also be analytically derived through considerations based on the eigenvalues associated with Osher's method. This prevents any perturbation of the downstream region to affect the upstream flow (the gradient of the numerical flux function on the shock interface with respect to the downstream state becomes zero) and thus suppresses errors in the upstream cell column adjacent to the shock. The inverse order version of Osher's scheme does not present these features and remains unstable.

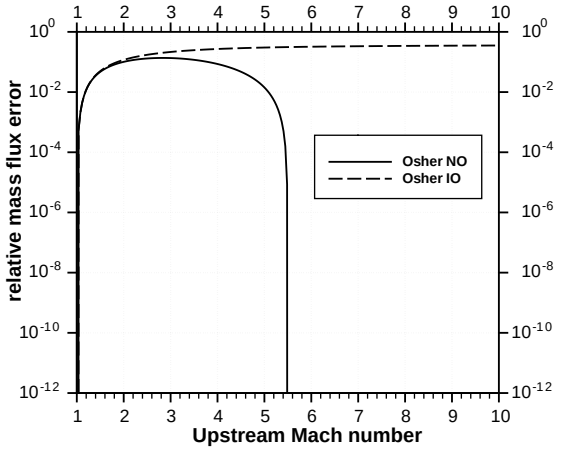

Fig. 12. Different behavior of the two versions of Osher's scheme on the thin steady shock.

4.5. Bifurcation mechanism towards the carbuncle solution in the blunt body problem

Given the dependence of the carbuncle on various parameters like the upstream Mach number and the form factor, it is now much easier to understand the bifurcation mechanism which leads to the carbuncle solution in blunt body calculations. As the bow shock ahead of the blunt body reaches a steady position during the integration process, the combination of parameters (M_0, α_ρ) may lead to unconditional instability according to Fig. 8. The expected solution of a strong detached normal bow shock is prevented and the numerical fluid has to seek another solution: the carbuncle. We recall Lax's theorem which states that a

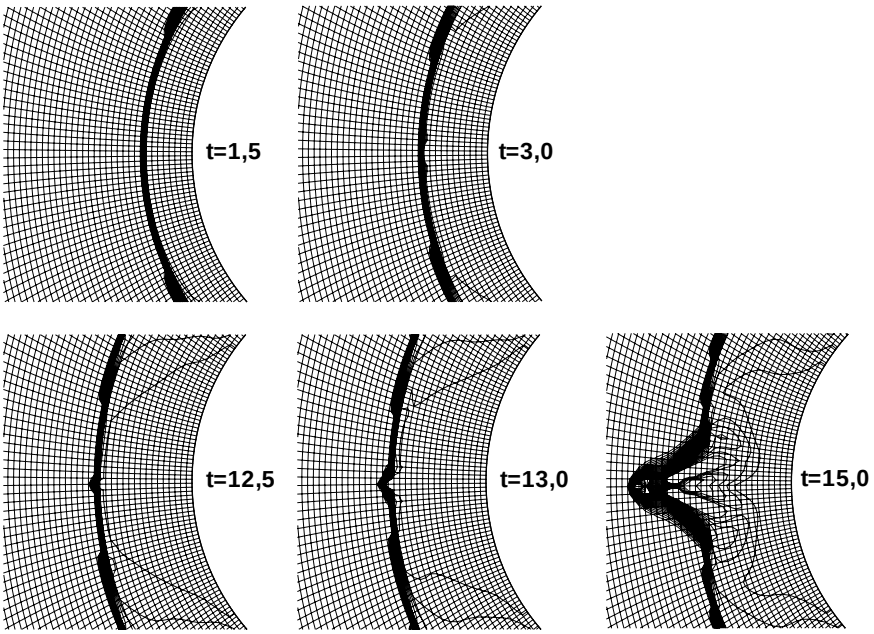

numerical scheme only converges if it is consistent and stable. The onset of a carbuncle solution and the bifurcation to the complex shock pattern originating from the (unstable) normal bow shock can be seen in Fig. 13.

With Fig. 8 it is also possible to explain another behavior of the carbuncle observed in blunt body calculations. If the first iterations (so that the bow-shock reaches its final position) are done with a stable scheme like EFM, which automatically thickens shocks, and then the calculation is carried on with Roe's scheme, it is possible to observe either a stable or an unstable shock wave, depending on the grid and the upstream Mach number used. The notions of convexity and concavity illustrated in Fig. 8 allow to determine in advance whether an EFM precalculated solution will remain stable (for a stable convex shock) or if it will destabilize (in the unstable concave case).

5. Conclusions

- The stability analysis method presented in this paper clearly showed an unconditional instability with exponential error growth in certain shock configurations of the following schemes: *Godunov*, *Roe*, *Osher*, *HLLEM*. The instability is unconditional because our analysis is continuous in time and thus the result is independent of the CFL number and even independent of the time discretization technique since only the spatial discretization operator is analyzed.
- The present method is able to retrieve the typical sawtooth form along with the Jordan form of the unstable mode directly from the discretized Euler equations, without making any a priori assumptions on a particular form of the unstable mode.
- The method predicts a threshold of the upstream Mach number which triggers the instability, in good agreement with computations, when numerical fluxes are differentiable. For non-differentiable fluxes, the actual averaging evaluation needs to be improved.
- The matrix stability analysis revealed that the numerical shock structure is an important parameter which greatly influences the carbuncle phenomenon. Indeed, highly convex shocks computed with Roe's scheme remain stable for extremely high values of the upstream Mach number.
- It could be shown in Section 4.4 that the shock instability originates in the upstream region and this instability is then convected downstream to produce the mode mainly visible downstream, as shown in Fig. 4. This explains why shock-fitting techniques never produce instabilities on the blunt body problem.
- The concentration of the source of the carbuncle in the small cell column region upstream the shock explains the effectiveness of the selective dissipation correction proposed by Liou [28], where additional transversal dissipation is only applied if the local normal Mach number crosses 1.

One drawback of the present method is that the eigenvalues of S cannot be calculated analytically because of the large dimension of S. So the destabilizing terms in each scheme cannot be directly identified. However, since for extremely high upstream Mach numbers, steady (concave) shock waves can go unstable and the equations become insensitive to the Mach number, some analytical calculations could be done in the limit $M_0 \to \infty$. Further investigations are also needed to better understand in what situations convex shocks appear rather than concave ones.

References

[1] K.M. Peery, S.T. Imlay, Blunt body flow simulations, AIAA Paper 88-2924, 1988.
[2] J. Quirk, A contribution to the great Riemann solver debate, International Journal of Numerical Methods in Fluids 18 (6) (1994) 555–574.
[3] J. Gressier, Robustesse et Précision des Schémas Décentrés pour les Ecoulements Compressibles, Ph.D. Thesis, No. 285, SUPAERO, Toulouse, France, 1999.

[4] R. Walder, Some aspects of the computational dynamics of colliding flows in astrophysical nebulae, Ph.D. Thesis, Astronomy Institute, ETH-Zürich, No.10302, 1993.
[5] S. Bogdonoff, I.E. Vas, Preliminary investigation of spiked bodies at supersonic speeds, Journal of the Aeronautical Science 26 (1959) 584–594.
[6] A.G. Panaras, Pulsating flows about axisymmetric concave bodies, AIAA Journal 19 (6) (1981) 804–806.
[7] J.P. Finley, The flow of a jet from a body opposing a supersonic free stream, Journal of Fluid Mechanics 26 (1966) 337–368.
[8] B. Meyer, H.F. Nelson, D.W. Riggins, Hypersonic drag and heat-transfer reduction using forward-facing jet, Journal of Aircraft 38 (4) (2001) 680–686.
[9] S. Aso, K. Hayashi, M. Mizoguchi, A study on aerodynamic heating reduction due to opposing jet in hypersonic flow, AIAA Paper 2002-0646, 2002.
[10] M. Holden, Studies of boundary layer transition and surface roughness effects in hypersonic flow, CALSPAN Report 6430-A-5, 1983.
[11] D. Riggins, H.F. Nelson, E. Johnson, Blunt-body wave drag reduction using focused energy deposition, AIAA Journal 37 (4) (1999) 460–467.
[12] R.M. Bracken, L.N. Myrabo, H.T. Nagamatsu, M.N. Shneider, Y.P. Raizer, Experimental investigations of an 'Air Spike' with and without blunt body in hypersonic flow, AIAA Paper 2001-0796, 2001.
[13] S.P. Kuo, D. Bivolaru, Plasma effects on shock waves in a supersonic flow, Physics of Plasmas 8 (7) (2001) 3258–3264.
[14] J.-Ch. Robinet, J. Gressier, G. Casalis, J.-M. Moschetta, Shock wave instability and carbuncle phenomenon: same intrinsic origin?, Journal of Fluid Mechanics 417 (2000) 237–263.
[15] A. Harten, High resolution schemes for hyperbolic conservation laws, Journal of Computational Physics 49 (1983) 357.
[16] H.-C. Lin, Dissipation additions to flux-difference splitting, Journal of Computational Physics 117 (1995) 20–27.
[17] J. Gressier, J.-M. Moschetta, Robustness versus accuracy in shock-wave computations, International Journal of Numerical Methods in Fluids 33 (2000) 313–332.
[18] L. Flandrin, P. Charrier, B. Dubroca, A robust finite-volume method for computations of two-dimensional unstructured hybrid meshes, in: S. Wagner, E.H. Hirschel, J. Périaux, R. Piva (Eds.), Computational Fluid Dynamics'94, Wiley, New York, 1994, pp. 301–308.
[19] K. Sermeus, H. Deconinck, Solution of steady Euler and Navier–Stokes equations using residual distribution schemes, in: 33rd Computational Fluid Dynamics Course, VKI Lecture Series 2003-05, 2003.
[20] K. Xu, Gas evolution dynamics in Godunov-type schemes and analysis of numerical shock instability, NASA/CR-1999-208985 ICASE Report No. 99-6, 1999.
[21] J.-M. Moschetta, J. Gressier, J.-C. Robinet, G. Casalis, The carbuncle phenomenon: a genuine Euler instability?, in: E.F. Toro (Ed.), Godunov Methods, Theory and Applications, Kluwer Academic/Plenum Publishers, 1995, pp. 639–645.
[22] R. Sanders, E. Morano, M.-C. Druguet, Multidimensional dissipation for upwind schemes: stability and applications to gas dynamics, Journal of Computational Physics 145 (1998) 511–537.
[23] M. Pandolfi, D. D'Ambrosio, Numerical instabilities in upwind methods: analysis and cures for the carbuncle phenomenon, Journal of Computational Physics 166 (2001) 271–301.
[24] Y. Wada, M.-S. Liou, An accurate and robust flux splitting scheme for shock and contact discontinuities, SIAM Journal of Scientific Computation 18 (3) (1997) 633–657.
[25] J. Gressier, P. Villedieu, J.-M. Moschetta, Positivity of flux vector splitting schemes, Journal of Computational Physics 155 (1999) 199–220.
[26] E.F. Toro, M. Spruce, W. Speares, Restoration of the contact surface in the HLL-Riemann solver, Shock Waves 4 (1994) 25–34.
[27] P. Batten, N. Clarke, C. Lambert, M.D. Causon, On the choice of waves speeds for the HLLC Riemann solver, SIAM Journal of Scientific Computation 18 (6) (1997) 1553–1570.
[28] M.-S. Liou, Mass flux schemes and connection to shock instability, Journal of Computational Physics 160 (2000) 623–648.
[29] J.R. Edwards, A low-diffusion flux-splitting scheme for Navier–Stokes calculations, Computers and Fluids 26 (6) (1997) 635–659.
[30] F. Coquel, M.S. Liou, Hybrid Upwind Splitting (HUS) by a field by field decomposition, NASA TM-106843, 1995.
[31] D.I. Pullin, Direct simulation methods for compressible inviscid ideal gas flow, Journal of Computational Physics 34 (1980) 231–244.
[32] K.H. Kim, C. Kim, O.-H. Rho, Methods for the accurate computations of hypersonic flows, I. AUSMPW+ scheme, Journal of Computational Physics 174 (2001) 38–80.
[33] K.H. Kim, C. Kim, O.-H. Rho, Cure for shock instability: development of an improved Roe scheme, AIAA Paper 2002-0548, 2002.
[34] M.N. Macrossan, R.I. Oliver, A kinetic theory solution method for the Navier–Stokes equations, International Journal of Numerical Methods in Fluids 17 (1993) 177–193.
[35] J.-M. Moschetta, Mass flux computation as a key to the carbuncle phenomenon, in: E.F. Toro (Ed.), Godunov Methods, Theory and Applications, Kluwer Academic/Plenum Publishers, 2001, pp. 623–629.

[36] K. Xu, Z. Li, Dissipative mechanism in Godunov-type schemes, International Journal of Numerical Methods in Fluids 37 (2001) 1–22.
[37] B. Einfeldt, C.D. Munz, P.L. Roe, B. Sjogreen, On Godunov-type methods near low densities, Journal of Computational Physics 92 (1991) 273–295.
[38] A. Gelb, Applied Optimal Estimation, MIT Press, Cambridge, 1974.
[39] C. Hirsch (Ed.), Numerical Computation of Internal and External Flows, vol. 1, Wiley, New York, 1991.